Monitoring Spatial and Temporal Patterns of Rubber Plantation Dynamics Using Time-Series Landsat Images and Google Earth Engine

Yuchen Li, Chenli Liu, Jun Zhang, Ping Zhang, and Yufei Xue

***Abstract*—Rubber plantation is an important strategic material related to the national economy and people's livelihoods. Up-to-date and accurate rubber plantation maps are critical for monitoring the area and spatial distribution of rubber plantations and assessing their impacts on society, the economy, and the environment. However, existing optical images are greatly limited by frequent cloud cover, which seriously affects the accuracy of rubber plantation area extraction. To overcome this issue, we used dense Landsat time series stacks based on Google Earth Engine, combined phenological features, and applied random forest algorithms to monitor rubber plantations in Xishuangbanna from 1987 to 2020. The results showed that 1) the phenological characteristics of rubber plantations in Xishuangbanna indicated that the leaf-off period lasts from late December to mid-February of the following year, while the leaf-on of rubber plantations occurred in other months; 2) the overall accuracy and kappa coefficient values ranged from 0.82 to 0.96 and 0.76 to 0.95, respectively, showing that the extraction accuracy of rubber plantation information can meet the accuracy requirement; 3) the rubber plantation area in Xishuangbanna increased between 1987 and 2020 from 7.05×10^4 to 47.78×10^4 hm^2. The peak rubber plantation area occurred in 2015 (49.60×10^4 hm^2) followed by a downward trend; 4) spatially, the rubber plantation is mainly distributed in Jinghong City and Mengla County, while less abundant in Menghai County. Overall, this article is expected to contribute to the rapid and accurate mapping of rubber plantations in large-scale applications and analysis.**

***Index Terms*—Google Earth Engine (GEE), phenology, random forest (RF), rubber plantation, Xishuangbanna.**

I. Introduction

RUBBER plantation (*Hevea brasiliensis*) is hailed as one of the four major industrial raw materials in the world [1]. As an important economic crop and the only renewable green energy raw material, it has become an indispensable strategic energy source for China's national defense and industrial construction. With the steady development of the economy, natural rubber plays an increasingly important role in China's national economy [2]. Due to the suitable climate and growing conditions, Southeast Asia and southern China have the largest number of rubber plantations in the world [3], [4]. In recent years, with the increasing global demand for natural rubber products, the area of rubber plantations has expanded dramatically. As one of the main rubber planting areas, Xishuangbanna in southern China has undergone an extensive and dramatic expansion in the area occupied by rubber plantations in the past decades [5]. Large-scale rubber planting has increased the income of local governments and farmers, but it has also caused many ecological and environmental problems, such as the dramatic reduction of tropical rain forests and loss of biodiversity [6]. Therefore, to obtain a clearer understanding of the local rubber planting situation, accurate mapping of the temporal and spatial changes of rubber plantations in Xishuangbanna is urgently needed to provide support for decision-making concerning economic development and ecological protection.

The development of remote sensing makes satellite-based imagery an effective means of monitoring rubber plantation changes [7]. Recently, many scholars have conducted extensive research on extracting rubber plantation information from remote sensing data. For example, Liao *et al*. [8] used Landsat data to monitor rubber plantations in Xishuangbanna by remote sensing. Liu *et al*. [9] used an object-oriented method to analyze the temporal and spatial distribution characteristics of Xishuangbanna rubber plantations. Gao *et al*. [10] used spatial–temporal fusion algorithms, selecting ETM+, OLI, Sentinel-2 data at medium resolution, and MODIS data at high temporal resolution to establish a high spatial–temporal resolution visible remote sensing dataset, achieving high accuracy. However, these studies of rubber plantations are only based on spectral characteristics of single-phase data in the extraction time window. Furthermore, rubber plantations grow in tropical rainforest areas with complex ecosystems and are characterized by high vegetation coverage, so they have spectral characteristics similar to those of natural forests [11]. These problems produce large uncertainties in extraction monitoring of rubber planting. To overcome this drawback, Liu *et al*. [9] combined the interannual defoliating and foliating features of rubber trees as a method to monitor rubber

Manuscript received May 4, 2021; revised July 12, 2021; accepted August 31, 2021. Date of publication September 8, 2021; date of current version September 30, 2021. This work was supported in part by the Project of Innovative Talents Cultivation for Graduate Students of Yunnan University: Construction of Graduate Tutor Team — Regional Water and Soil Resources, Environmental Evolution and Regulation, Grant Number (C176230200), and the Project of First-class Discipline Construction of Yunnan University Geography (C176210215). *(Corresponding author: Jun Zhang.)*

Yuchen Li, Jun Zhang, Ping Zhang, and Yufei Xue are with the School of Earth Sciences, Yunnan University, Kunming 650500, China (e-mail: feiyu0061@gmail.com; zhjun@ynu.edu.cn; zhangping2720@163.com; nidhoggx@126.com).

Chenli Liu is with the State Key Laboratory of Grassland Agro-Ecosystems, Key Laboratory of Grassland Livestock Industry Innovation, Ministry of Agriculture and Rural Affairs, Engineering Research Center of Grassland Industry, Ministry of Education, College of Pastoral Agriculture Science and Technology, Lanzhou University, Lanzhou 730000, China (e-mail: liuchl18@lzu.edu.cn).

Digital Object Identifier 10.1109/JSTARS.2021.3110763

plantations. Fan *et al.* [12] compared the extraction accuracy of rubber plantations from different phenological indexes in Xishuangbanna. Overall classification accuracies derived from normalized difference vegetation index (NDVI) were 93%, with corresponding Kappa coefficient of 0.86. Therefore, the use of multitemporal remote sensing images to monitor crops and to obtain planting information on a large scale has been widely applied to the growth monitoring and yield estimations of crops [13], [14].

However, severe weather conditions make it difficult to obtain cloudless single-scene Landsat images, which limits the ability of Landsat data to monitor rubber plantation changes in Xishuangbanna. To resolve this issue, the dense time stack method overlays all available Landsat images and replaces the area covered by clouds by stacking the coverage from another image [15], [16]. The approach can effectively overcome the cloud cover challenge and generate a high-quality image. However, managing large volumes of satellite imagery for large-scale analysis is a huge challenge when using traditional remote sensing methods based on workstation PC systems and commercial imaging processing software [17]. Thus, we need a comprehensive solution to meet the needs of remote sensing applications. Cloud computing platforms are an effective way to store, access, and analyze data sets on very powerful servers. Google Earth Engine (GEE) is a web-based remote sensing data processing cloud platform, which can rapidly realize the processing and visualization for massive remote sensing datasets, and which is widely used to investigate various pressing social issues [18], [19]. Some studies have used GEE to map long-term series or large-scale land cover, sugarcane planting, and wetlands changes [15], [20], [21]. However, to our knowledge, no previous studies have used dense time stacks of Landsat images on the GEE platform to monitor temporal and spatial changes in rubber plantations.

Given the above discussion here, this article used time-series Landsat images and the GEE platform to map rubber plantations as a specific class, independent of other major land-cover categories, over large areas. The main objectives of this article were to 1) investigate the rubber plantation phenology in Xishuangbanna and explore the time window of information extraction, 2) explore the potential for combining Landsat data with random forest (RF) methods in rubber plantation areas to map the rubber plantation distribution across this region during 1987–2020 and to evaluate the accuracy of maps, and 3) analyze the spatiotemporal change patterns of rubber plantations in Xishuangbanna. The results generated in this article will be beneficial to help local managers formulate reasonable rubber plantation resource management strategies, and at the same time provide some guidance for similar research in China.

II. Study Area and Data

A. Study Area

Xishuangbanna Dai Autonomous Prefecture is located in Yunnan Province in southwest China and in the middle and upper reaches of the Lancang–Mekong River, between 21°08′∼22°36′N and 98°56′∼101°50′E (see Fig. 1). It is the northernmost tropical rainforest in Southeast Asia and an important tropical forest area in China. This region, south of the Tropic of Cancer, belongs to a tropical monsoon climate zone. The annual average temperature of the whole state is between 10.9°C and 22.6°C. November–April is the dry season, and May–October is the rainy season. The annual average precipitation is 1250 to 3750 mm, and the annual total sunshine hours is 2000 h [22]. The topography is dominated by mountains separated by vast valleys and basins. The terrain is gradually inclined from north to south, with relatively high elevation on the southern edge. The structural integrity of forest ecosystems in the study area, and the forest ecosystem is highly diverse and the vegetation types are rich and grow abundantly, with subalpine vegetation, mid-low mountain vegetation, and monsoon forest vegetation showing horizontal and vertical zonal distribution. The area is rich biodiversity and good climatic conditions. Policies encouraging rubber planting over the past several decades have led to widely-distributed rubber cultivation in Xishuangbanna [4], which has contributed to the gradual decline of local species diversity.

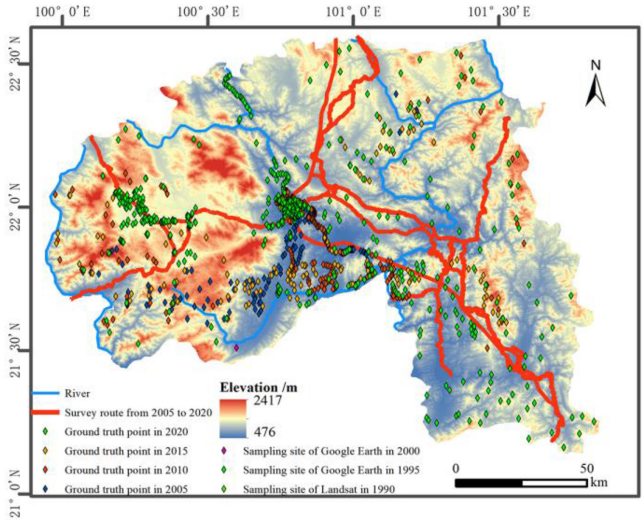

Fig. 1. Geographic location of the study region.

B. Landsat Imagery

In this article, we collected the surface reflectance of Landsat-5/7/8 from the United States Geological Survey.[1] The Landsat imageries of Xishuangbanna is covered by five Worldwide Reference System (WRS-2) paths/rows (130/44, 130/45, 131/44, 131/45, 129/45) [see Fig. 2(a)]. From 1987 to 2020, there were 2230 Landsat images, 789 Landsat-5 images, 710 Landsat-7 images, and 731 Landsat-8 images available in the research area. In order to obtain high-quality images, the Landsat image with cloud cover more than 47% were removed, and a total of 1583 images were used through GEE in this article. The analysis showed that there are many good observations in January–April and November–December, with 1212 images, while there are relatively few good observations in May–October, with only

[1][Online]. Available: https://earthexplorer.usgs.gov/

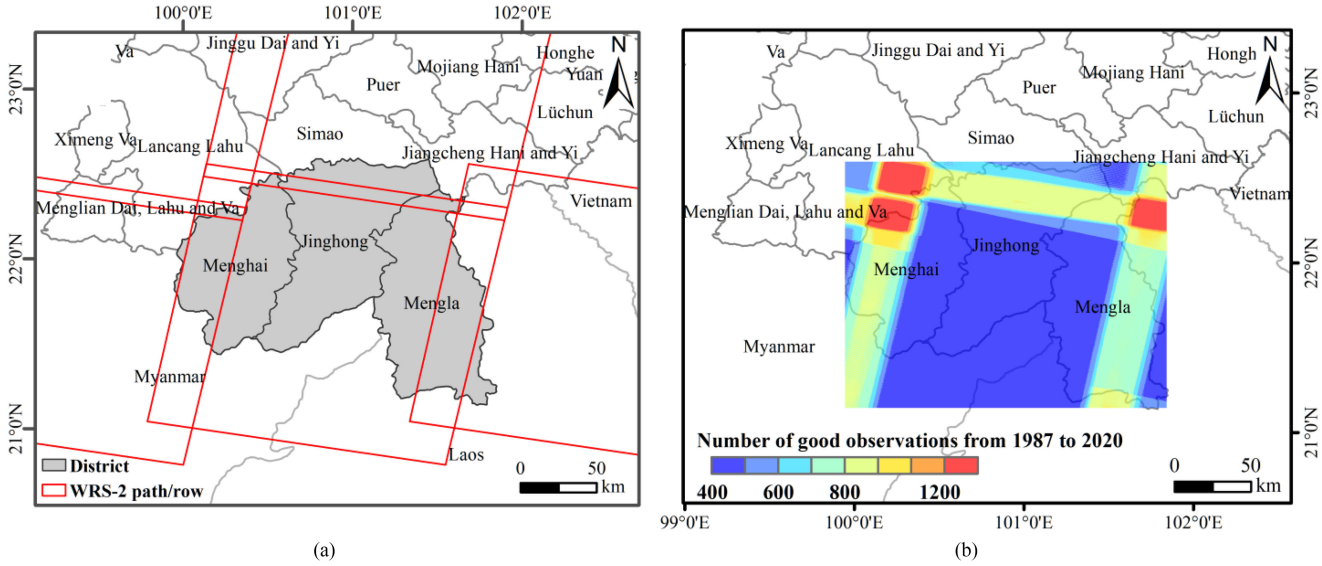

Fig. 2. (a) Spatial distribution of the Xishuangbanna zone and Landsat WRS-2 path/rows in China, and (b) spatial distribution of the number of from good-quality observations within individual pixels of landsat 5/7/8 images from 1987 to 2020.

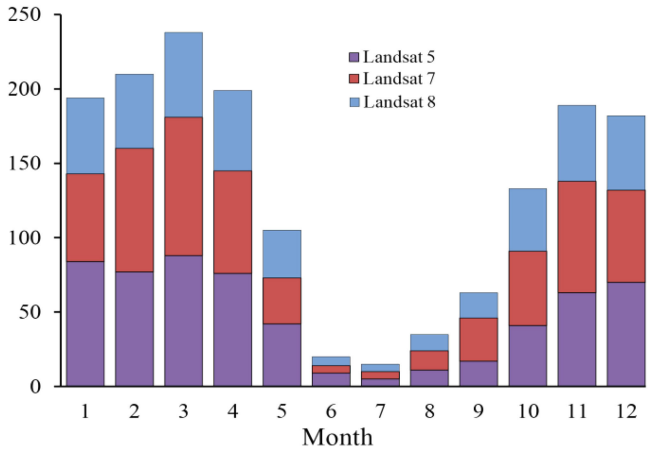

Fig. 3. Distribution of Landsat 5, 7, and 8 images in different months from 1987 to 2020.

371 images [see Fig. 2(b)]. By analyzing the distribution of data in different months, it was found that the data in the study area had obvious seasonality, as shown in Fig. 3. Moreover, the digital elevation model data from the Space Shuttle Radar Terrain Mission were then used to identify and eliminate terrain shadows by GEE.

C. Ground Reference Data and Sample Points

The determination of characteristic parameters of different land cover types is the key to classification accuracy [23]. Compared with evergreen broad-leaf forest, rubber plantation vegetation is often difficult to identify visually in remote sensing images. Therefore, it is necessary for us to ensure a sufficient number and quality of sample points for classification and accuracy validation. From 2005 to 2020, randomly extensive field investigations were conducted near the survey route from

TABLE I
NUMBER OF SAMPLE POINTS FROM 1987 TO 2020

Year	Land cover type				
	Rubber plantation	Forest land	Water body	Construction land	Farmland
1987	50	50	12	20	27
1990	50	67	17	38	30
1995	75	64	16	40	29
2000	65	56	20	36	31
2005	93	90	15	40	38
2010	104	100	19	35	32
2015	87	90	21	39	37
2020	96	112	24	56	47

January to April and from October to December every year. We randomly chose points that were more than 1500 m apart to minimize spatial homogeneity [15], [24]. The location, district, and Land use/land cover (LULC) information were acquired from the Mobile GIS. After screening, 1544 typical sample points of surface cover data were obtained in the field. In addition, 422 representative and typical pure pixels were visually interpreted in the images of Google Earth map and related years as training sample data points [23]. A total of 620 rubber plantation sampling points, 144 water bodies, 629 forest land, 304 construction land, and 271 farmlands areas were selected (see Fig. 1). The detailed sample data is shown in Table I. In this article, two out of three sample points in each of the years from 1987 to 2020 were randomly selected to construct the classification model, 1/3 samples from each year were used to calculate the confusion matrix to evaluate the accuracy of the classification results [25].

III. METHODOLOGY

In this article, the method to map rubber plantations in Xishuangbanna includes four steps (see Fig. 4). First, image preprocessing was performed to generate monthly time-series

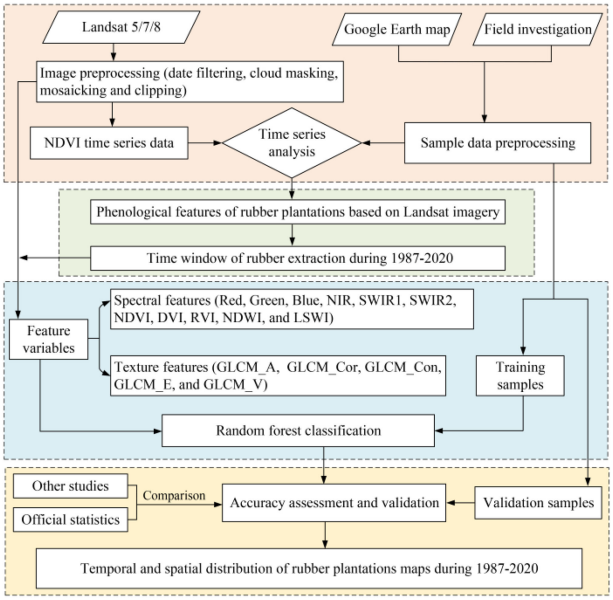

Fig. 4. Workflow for mapping rubber plantations through landsat and phenology.

data and collect training samples. Second, the rubber extraction window was determined using the time-series NDVI. Third, classification feature parameters were constructed and RF algorithm classification was applied. Finally, the results were validated using a confusion matrix and statistical data, and spatial distribution information of rubber plantations was mapped.

A. Phenological Features of Rubber Plantations Based on Landsat Imagery

Phenology is a periodic response of organisms to the environment, such as leaf growth, flowering, fruiting, and deciduous leaf loss within a year, which provides a comprehensive reflection of the meteorological conditions at that time and in the past [26], [27]. During the field investigation in the research area, we observed that the canopy of the rubber plantation underwent obvious changes. First, the rubber trees began to enter the leaf-off period in December, and the leaves became yellow due to low-temperature dormancy. Then, in late February, the rubber trees entered the first awning leaf emergence period, where new leaves gradually sprouted and green leaves were gradually restored in the canopy [28]. It could thus be seen that the significant phenological changes of rubber trees were directly reflected in leaf emergence and litterfall in the study area. Rubber trees can be easily identified by color and texture during this process. Therefore, changes in leaf litter and the new initiation of rubber planting provide a physiological basis for rubber plantation identification. NDVI can be used to determine the optimal window for rubber plantation extraction if it is expressed in the remote sensing images.

B. Construction of Rubber Plantations Classification Features

1) Spectral Features: When using preprocessed images to calculate classification parameters, the target land types in the study area should be considered first. According to the LULC in the study area, this area can be divided into vegetation, nonvegetation, water, nonwater, artificial, and nonartificial land. In this article, we used five spectral indices to identify and distinguish the aboveground cover.

In order to eliminate nonvegetation, NDVI is selected in this article, which is a band combination composed of the reflectance difference between vegetation and other land covers in the Red and NIR bands. This index can provide information about the parameters of crop growth, type, and vegetation distribution [29]. Therefore, this index can also be used to reflect vegetation growth and vegetation density. The formula used in this article is

$$\mathrm{NDVI} = \frac{\mathrm{NIR} - \mathrm{Red}}{\mathrm{NIR} + \mathrm{Red}}. \tag{1}$$

The differential vegetation index (DVI) is extremely sensitive to changes in soil background, which can eliminate the influence of soil background [30]. The DVI index is the difference between the near-infrared band and visible red band and is given by

$$\mathrm{DVI} = B5 - B4. \tag{2}$$

In addition, the visible spectra of red light and near-infrared have different spectral responses to green plants. We therefore used the approach of [31] to propose the ratio vegetation index (RVI), which takes advantage of the differential reflectance of sunlight through the canopy in the NIR and Red bands. The RVI is calculated as follows:

$$\mathrm{RVI} = \frac{\mathrm{NIR}}{R}. \tag{3}$$

In order to eliminate water bodies, a normalized difference water index (NDWI) is selected in this article, which can effectively suppress other types of land cover and highlight water information through band combination [32]. The NDWI is calculated as follows:

$$\mathrm{NDWI} = \frac{\mathrm{Green} - \mathrm{NIR}}{\mathrm{Green} + \mathrm{NIR}}. \tag{4}$$

By analyzing the spectral information of the ground objects, it is found that the reflectance values of the ground objects in the NIR band and SWIR-1 band are scattered during the leaf-off phase, which can reflect the water in vegetation and soil well. Therefore, in this article, the land surface water index (LSWI) is sensitive to soil moisture and soil water content and is used to distinguish rubber trees from other types of vegetation [33], [34]. The concrete calculation method is as follows:

$$\mathrm{LSWI} = \frac{\mathrm{NIR} - \mathrm{SWIR1}}{\mathrm{NIR} + \mathrm{SWIR1}}. \tag{5}$$

2) Texture Features: Texture features refer to the fact that the color and gray level of ground objects change to a certain extent, showing irregular changes locally on the map but showing regular patches at larger scales [35]. However, the texture characteristics of rubber plantations in the leaf-off period are obvious, which can make up for defects of misclassification and misjudgment based solely on spectral information and improve the classification accuracy. Therefore, this article studies the selection of angular second moment, correlation, contrast, entropy,

and variance features of the gray-level co-occurrence matrix (GLCM) when obtaining texture features in the Red, Green, and Blue bands of the leaf-off period [36]. Texture features that are considered to provide good classifications in remote sensing are analyzed. The window size is 5×5 pixels, which is generated for each pixel and its neighborhood in the horizontal direction [37].

The angular second-order moment of GLCM is a measure of the uniformity of the grayscale distribution of the image. When the information distribution in the image is concentrated near the main diagonal, it shows that the information distribution of the image is uniform, and its value is large. Conversely, if all the values of the GLCM of image information are equal, the information distribution value is small. The angular second-order moment can be calculated using the following equation:

$$\mathrm{GLCM_A} = \sum_{i=0}^{\mathrm{quant}_k} \sum_{j=0}^{\mathrm{quant}_k} p(i,j)^2. \tag{6}$$

GLCM_Cor is a parameter describing the similarity between the elements in the row or column of the GLCM, which reflects the extension length of its characteristic gray level in a certain direction. The longer the extended length, the greater the correlation. GLCM_Cor is applied to measure the linear relationship of grayscale data, using the equation:

$$\mathrm{GLCM\_Cor} = \sum_{i=0}^{\mathrm{quant}_k} \sum_{j=0}^{\mathrm{quant}_k} \frac{(i-\mathrm{mean}) * (j-\mathrm{mean}) * p(i,j)^2}{\mathrm{variance}}. \tag{7}$$

GLCM_Con is a parameter reflecting the total amount of local gray level changes: the larger the gray-level difference, the greater the image contrast, and the clearer the visual effect. It is defined as follows:

$$\mathrm{GLCM_{Con}} = \sum_{i=0}^{\mathrm{quant}_k} \sum_{j=0}^{\mathrm{quant}_k} p(i,j)^2 * (i-j)^2. \tag{8}$$

GLCM_E is a measure of information degree in an image and a characteristic parameter for measuring the randomness of gray-level distribution, which indicates the complexity of the texture in an image. The more complex the texture, the greater the entropy, while the more uniform the gray level, the smaller the entropy. It is calculated according to the following equation:

$$\mathrm{GLCM\_E} = -\sum_{i=0}^{\mathrm{quant}_k} \sum_{j=0}^{\mathrm{quant}_k} p(i,j) * \ln p(i,j). \tag{9}$$

GLCM_V can reflect the measure of deviation between pixel value and mean value. When the gray level changes greatly in the image, the variance is larger. It is calculated according to the following equation:

$$\mathrm{GLCM_V} = \sum_{i=0}^{\mathrm{quant}_k} \sum_{j=0}^{\mathrm{quant}_k} p(i,j)^2 * (i-\mathrm{mean})^2. \tag{10}$$

C. Random Forest Machine Learning Algorithm

We selected an RF machine learning algorithm because it integrated multiple decision trees through an integrated learning approach; its basic unit was also a single decision tree which could effectively avoid the influence of data noise and overfitting [15], [38], [39]. Furthermore, the RF algorithm can accurately predict the role of multiple explanatory variables, has a certain tolerance for outliers, and is also regarded as one of the best machine learning algorithms because of its small prediction error and fast operation [40], [41]. It operates on the main principle of drawing *n* samples from the original sample dataset and then modeling decision trees for each sample, combining multiple trees to make predictions, and finally voting to obtain the prediction results [42]. Thus, it can be said that RF is a meta-estimator for decision tree analysis based on a large number of subsamples, mainly using the mean to improve the accuracy of the prediction and to obtain the final prediction results without getting rid of the range of training samples. It can also be used for both regression and classification; classification is the main purpose of this article. After several experiments, the number of classification trees is set to 300 trees.

In addition, for the classification process with more parameters, in order to avoid data redundancy, we also apply RF to evaluate the importance of the textural and spectral parameters. We used the method of Bootstrap with high efficiency to evaluate the importance of parameters [43]–[45]. The parameter evaluation method is: 30% of the original data not selected in the sampling process is used as out-of-bag (OOB) data, and the importance evaluation is carried out by calculating the OOB error of each decision tree in the RF, adding noise interference randomly to the features of the OOB data samples [46]. If the accuracy of the OOB data is significantly reduced after adding noise randomly, it means that the features have a great influence on the classification results. The calculation is as follows [47]:

$$\mathrm{VI}\ (\mathrm{M_A}) = \frac{1}{N} \sum_{k=1}^{N} B_{n_t}^{M_A} - B_{O_t}^{M_A} \tag{11}$$

where $\mathrm{VI}(M_A)$ indicates the importance of the variable, *M* is the number of features in the sample, *N* is the number of trees in the decision tree, and $B_{O_t}^{M_A}$ is the error of the *t*th decision tree when the eigenvalue M_A is not added to the noise interference. $B_{n_t}^{M_A}$ is the error of the *t*th decision tree when noise interference is added to any eigenvalue M_A.

D. Accuracy Evaluation

Accuracy analysis can objectively evaluate whether the classification method can better extract the information for rubber plantings. A confusion matrix is generally used to evaluate the classification accuracy and reliability, and the overall accuracy and Kappa coefficient are the most widely used methods [48]. The Kappa coefficient can reflect the consistency of extraction results and the spatial distribution of real objects. Studies have shown that when the Kappa coefficient is less than 0.4, the consistency is less than ideal. The consistency between the reference classification results and the rubber plantation extraction results

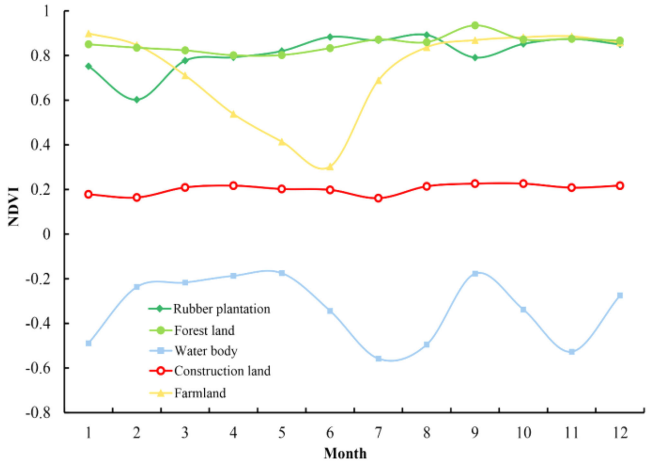

Fig. 5. Time-series plot of monthly mean NDVI based on landsat 8 images.

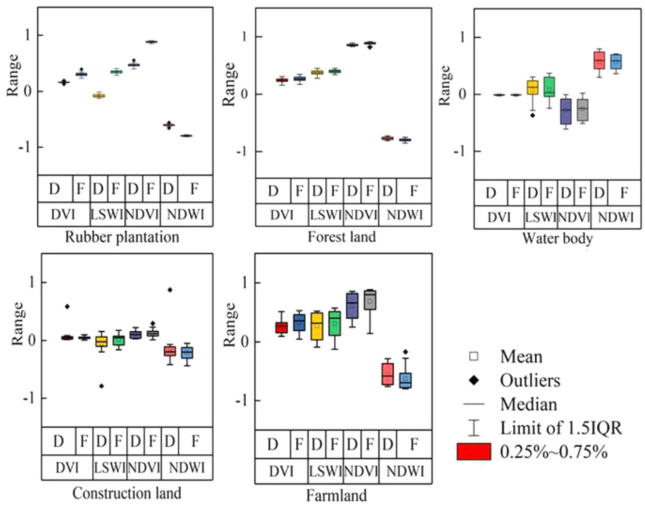

Fig. 6. Boxplots of DVI, LSWI, NDVI, and NDWI were calculated from the landsat imagery for leaf-off (D) and leaf-on (F) periods.

was relatively good when the Kappa coefficient was within the range of 0.40 to 0.60 [49], [50]. The rubber extraction effect can be evaluated for accuracy by assessing the classification results. These were calculated according to the following equations:

$$\text{Overall accuracy} = \frac{\sum_{i=1}^{k} x_{ii}}{\text{x}} \tag{12}$$

$$\text{Kappa} = \frac{x\sum_{i=1}^{k} x_{ii} - \sum_{i=1}^{k} x_{j*}x_{*j}}{\text{x}} \tag{13}$$

where X_{ii} is the number in row i, the ith column of the confusion matrix is the total number of verified data sets, and x_i* and $\text{x}*_i$ are the total number of samples in the ith row and ith column of the confusion matrix.

IV. Results

A. NDVI Time-Series Analysis of Typical Ground Cover

Vegetation has different physiological characteristics at different stages. The growth cycle of rubber in the study area was analyzed, and the results showed that the first leaf-emergence period of rubber trees occurred from March to April, and the second leaf-emergence period occurred in May. At this time, rubber entered the summer flowering period, and the third leaf-emergence period was from July to August. In December, rubber trees began to lose leaves, which continued until February when a new flowering period began. Therefore, the obvious phenological changes of rubber trees are directly reflected in the germination and withering of leaves. According to the time series of different land cover types (see Fig. 5), in February, during the leaf-off period on rubber plantations, the NDVI time series curve showed a significant trough. However, the NDVI value of water remained below 0, and the NDVI value of buildings was stable at approximately 0.2. Farmland showed a trough in mid-June and then rose rapidly to around 0.8. Values for all other forest types remained at approximately 0.8. Thus, there are obvious differences in time-series data between rubber plantations and other land cover types. This feature is the primary characteristic of rubber plantations that differs from other vegetation covers. As a result, based on the good distribution of image observations, Landsat series data in February, representing leaf-off, can not only highlight the phenological characteristics of rubber plantings but also avoid the image quality degradation caused by cloudy and foggy weather in the rainy season.

B. Construction of the Extraction and Classification Model for Rubber Plantations

The spectral features of the ground in the study area were analyzed, and a classification parameter box diagram was constructed (see Fig. 6). It can be seen from the index statistics that, for the building land cover type, there is little difference between the parameters of leaf-off and leaf-on, and the NDVI value of leaf-on is about 0.1, which differs from its values for other land cover types such as water, farmland, forests, and rubber plantations. The DVI of agricultural land is mainly around 0.25, and it is difficult to distinguish the eigenvalues of this land type from woodland and rubber plantations. The NDVI of woodland is very high, reaching 0.8 at the stages of leaf dropping and green leaf growth. Because NDWI is mainly used for water extraction, we can note that the NDWI of water is obviously different from other surface covers through the sample points obtained from the field and Google Earth map; the NDWI is thus used for water removal in the study area in this experiment. In addition, the NDWI values of construction and agricultural land for leaf-on are quite different from that of rubber. Therefore, NDWI can also be used as a function to distinguish architecture, agriculture, and rubber planting. However, the LSWI index and NDVI index of rubber plantations are quite different for leaf-off and leaf-on. The LSWI values of rubber plantations primarily vary from -1 to 0 during leaf-off and from 0.2 to 0.4 during leaf-on. The NDVI value of rubber plantations is mainly between 0.2 and 0.6 in the leaf-off stage and about 0.8 in the leaf-on stage. However, other land cover types do not share this characteristic, so the NDVI value can be used to extract rubber plantations.

The texture features of typical ground covers show that the contrast, GLCM_A, and GLCM_V of rubber plantations are

TABLE II
TEXTURE FEATURES OF LAND COVER TYPE

Texture features	Land cover type				
	Rubber plantation	Forest land	Water body	Construction land	Farmland
GLCM_A	0.18	0.45	0.50	0.21	0.32
GLCM_Cor	0.16	0.10	0.08	0.03	-0.08
GLCM_Con	5.19	0.68	3.05	2.21	1.76
GLCM_E	1.88	1.04	0.95	1.70	1.33
GLCM_V	3.11	0.33	1.71	1.30	0.96

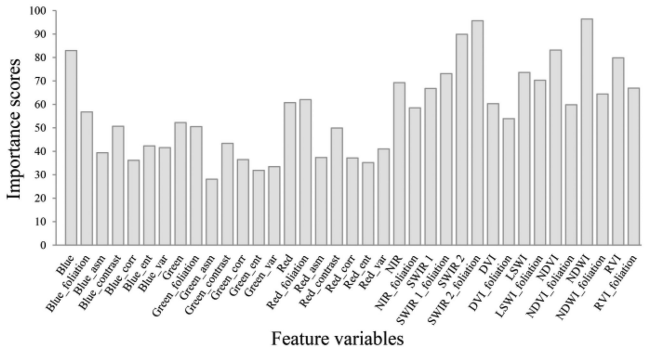

Fig. 7. Importance distribution of variables.

quite different from those of other land cover types (see Table II). The maximum GLCM_Con value of rubber plantations is 5.19, which is characterized by rich detail, obvious furrows, and high definition, indicating that rubber plantations provide abundant texture information. GLCM_A is smaller and shows a fine texture with a uniform distribution of image grayscale, which is easy to distinguishable from other forests. A larger rubber plantation GLCM_E shows a more complex texture compared to other land cover types. Rubber plantations have a GLCM_Cor value of 0.16, indicating a more directional texture relative to the rest of the land cover types. In addition, the rubber forest GLCM_V value is relatively high, which means that the grayness of the rubber forest is more variable and its texture is more periodic (see Table II).

C. Variable Importance Analysis and Accuracy Assessment

The RF can reduce data redundancy and processing workload by analyzing and evaluating the importance and contribution of feature variables to improve model accuracy. As shown in Fig. 7, the importance distribution of the variables obtained by OOB error analysis. The higher the importance score, the greater the influence and contribution of the variable to the classification results. The importance scores of NDWI and SWIR 2 in the green leaf phase were greater than 90, which was due to the fact that NDWI and the SWIR 2 band could suppress vegetation information and were more effective in discriminating soil moisture and prominent water bodies and distinguishing vegetation from water bodies and other surface cover. In contrast, the importance scores of texture features were all lower than 50, indicating that the contribution of texture features was lower than spectral features (see Fig. 7).

Accuracy assessment is a key component of map production using remote sensing data. Two out of three sample points in each of the years from 1987 to 2020 were randomly selected to construct the classification model, and all samples from each year were used to calculate the confusion matrix to evaluate the accuracy of the classification results. The accuracy verification results showed that the overall accuracy of the classification model from 1987 to 2020 was greater than 82%, and the Kappa coefficient was greater than 0.76 (see Table III). The classification accuracy was high, which showed that the accuracy of the classifier studied in this article and the consistency of spatial distribution reached a greater degree of accuracy.

D. Rubber Plantation Areas and Comparison With Statistics From Other Sources

Apart from evaluating the accuracy of the classification results, we calculate the area of rubber plantation classification. Rubber plantation area statistics generated from this article for Xishuangbanna that were compared with other sources such as the research of [9], [51], [52], and the Xishuangbanna Statistical Yearbook (see Table IV). We found that our statistical area was close to previous scholar's studies, but larger than the national statistical data, indicating that the rubber plantations in some areas had not yet been fully included in official statistics. However, Xiao *et al*. [53] reported lower values than those found in our study and values from statistical data.

E. Temporal and Spatial Distribution of Rubber Plantations

Our results show that the rubber plantation area has expanded since 1987 (see Fig. 8). Specifically, the areas of rubber plantations increased nearly septuple from 7.05×10^4 hm^2 in 1987 to 47.78×10^4 hm^2 in 2020. From the view of the county-level in Xishuangbanna, the increases in rubber plantation area are mainly distributed in Mengla County and Jinghong City, while the change in rubber plantation area in Menghai County is relatively small. The rubber plantation area of Mengla County and Jinghong City has grown rapidly: as of 2020, the total area of rubber plantations in Mengla County and Jinghong City has grown to 22.42×10^4 and 20.03×10^4 hm^2, respectively, but the area of rubber plantation in Menghai County has grown only to 5.34×10^4 hm^2.

Through analysis of the spatial distribution of rubber plantations, we can clearly see that the rubber plantations are mainly located in Mongla County and Jinghong City, accounting for more than 2/3 of the rubber plantations in Xishuangbanna, showing the spatial distribution characteristics of Jinghong City

TABLE III
USER'S ACCURACY (UA), PRODUCER'S ACCURACY (PA), OVERALL ACCURACY (OA), AND KAPPA COEFFICIENT FOR LAND COVER TYPE

Year	Accuracy	Land cover type					Index	
		Rubber plantation	Forest land	Water body	Construction land	Farmland	OA	Kappa
1987	UA	0.92	0.92	1.00	0.82	0.79	0.89	0.85
	PA	0.88	0.90	0.92	0.90	0.85		
1990	UA	0.83	0.94	1.00	1.00	1.00	0.95	0.93
	PA	1.00	0.89	1.00	1.00	0.95		
1995	UA	1.00	0.94	1.00	1.00	0.875	0.94	0.92
	PA	0.6	1.00	1.00	1.00	1.00		
2000	UA	0.97	0.98	0.93	0.95	0.89	0.96	0.95
	PA	0.94	0.98	1.00	0.80	0.95		
2005	UA	0.91	0.88	0.83	0.72	0.59	0.82	0.76
	PA	0.92	0.74	1.00	0.85	0.63		
2010	UA	0.93	0.88	0.84	0.88	0.61	0.86	0.80
	PA	0.91	0.81	0.84	0.83	0.84		
2015	UA	0.89	0.86	1.00	0.93	0.79	0.90	0.87
	PA	0.94	0.96	0.88	0.95	0.68		
2020	UA	0.94	0.90	1.00	0.96	0.91	0.94	0.92
	PA	0.95	0.95	1.00	0.95	0.90		

TABLE IV
RUBBER PLANTATION AREA COMPARISONS

	Year	This study	Liu *et al*. (2013) [9]	Liu *et al*. (2017) [51]	Xiao *et al*. (2019) [53]	Other studies	Official statistics *
Area (hm^2)	1987	7.05×10^4	–	–	3.31×10^4	–	–
	1990	12.03×10^4	12.84×10^4	–	5.24×10^4	–	8.50×10^4
	1995	14.92×10^4	–	–	6.37×10^4	–	–
	2000	19.77×10^4	25.80×10^4	–	8.95×10^4	20.03×10^4 [54]	13.20×10^4
	2005	33.52×10^4	–	30.36×10^4	13.55×10^4	–	19.00×10^4
	2010	44.38×10^4	50.10×10^4	47.33×10^4	21.94×10^4	49.00×10^4 [52]	27.13×10^4
	2015	49.60×10^4	–	50.04×10^4	22.90×10^4	–	30.17×10^4
	2020	47.78×10^4	–	–	–	–	29.80×10^4

Note: ∗Xishuangbanna Statistical Yearbook from http://www.xsbn.gov.cn/tjj/tjj.dhtml.

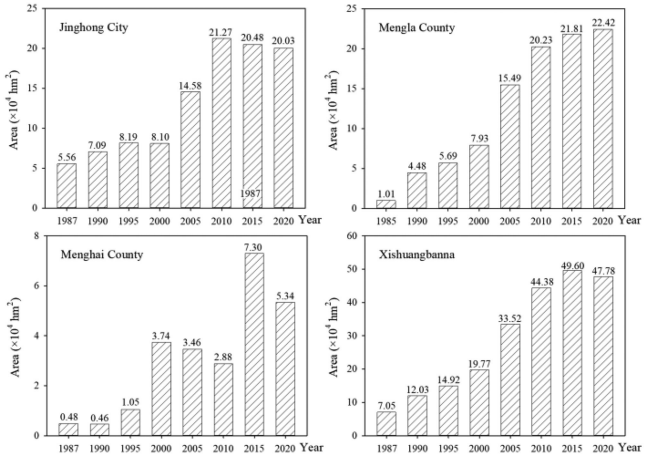

Fig. 8. Area of rubber plantations in Jinghong city, Mengla county, Menghai county, and Xishuangbanna from 1987 to 2020.

and Mengla County as the center (see Fig. 9). From 1976 to 2020, the area of rubber plantations was obviously increased in Jinghong City and Mengla County, while that in Menghai County had remained small there.

V. DISCUSSION

A. Selection of Variables Advantages of Monitoring Rubber Forest Using Phenology

Vegetation phenology is the most intuitive and sensitive biological index for seasonal and interannual changes in environmental conditions, and its changes can reflect the rapid response of terrestrial ecosystems to climate changes [55]. The phenological differences between rubber plantations and other vegetation types are an important factor affecting classification accuracy. Our results found that the rubber plants in Xishuangbanna began to lose leaves in late December until the middle of February, and the leaves showed significant changes from mid-February to late March. This finding is consistent with [12], probably due to the low temperature in the leaf-off period caused the crowns of the rubber trees to fall off [56], which caused the NDVI values of rubber trees in the remote sensing images to differ from those of other vegetation types during this period. In addition, the phenological ground observation showed that the biological rhythms of the rubber plantations and natural forest were distinctly different in Xishuangbanna [53]. However, compared to other traditional tropical rubber plantation areas such as Thailand and the Philippines with no obvious phenological characteristics or short durations of leaf-off, the

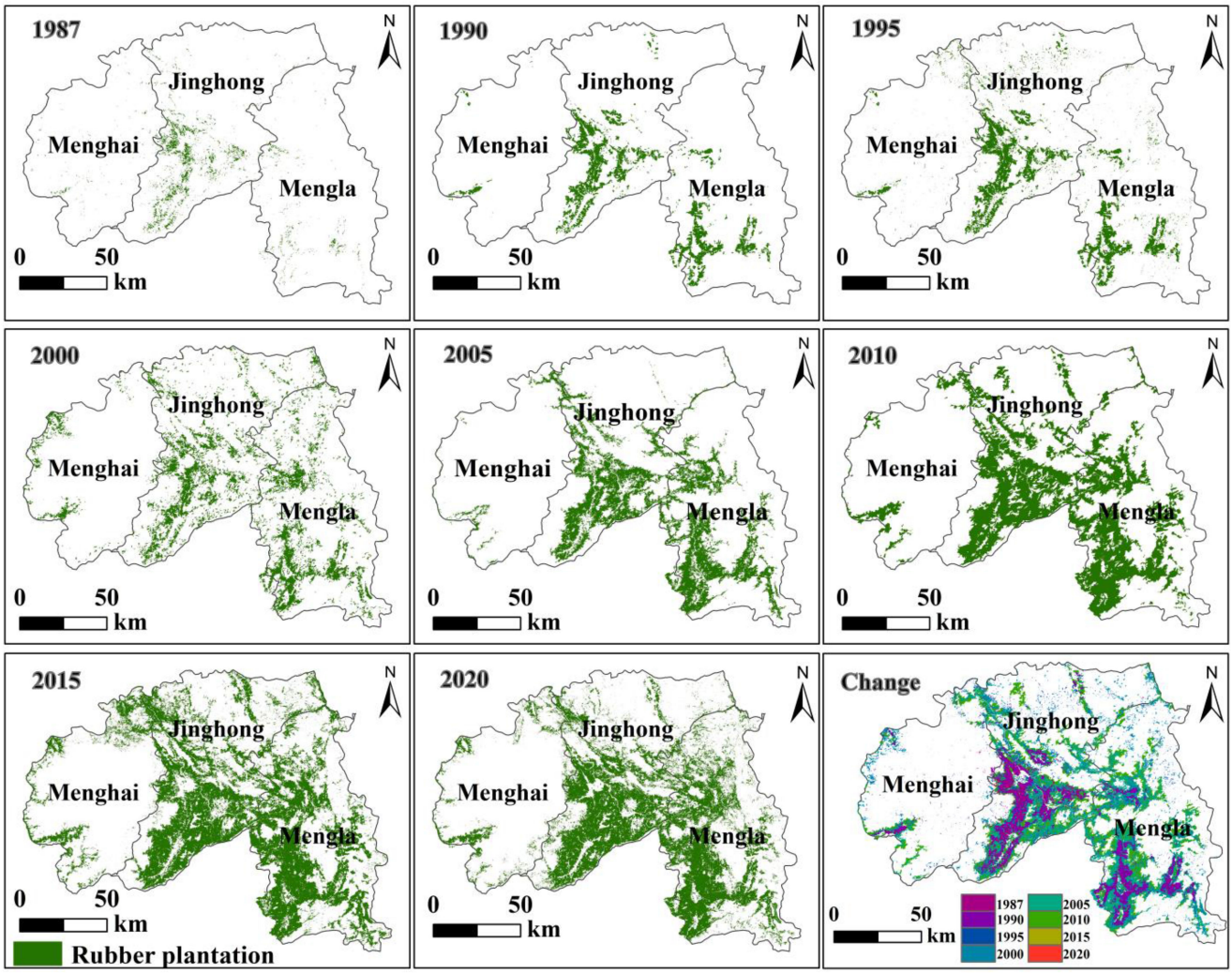

Fig. 9. Spatial distribution map of rubber planting in Xishuangbanna from 1987 to 2020. .

application of this method will be limited [57]. This further shows that the mapping of rubber plantations in the different region must consider the temporal inconsistency of the leaf-off and leaf-on of rubber plantations in different regions.

B. Spatial–Temporal Dynamic of Rubber Plantations in Xishuangbanna

The change of rubber plantation area is affected by the interaction of humans, the environment, and policies on different temporal and spatial scales. Accurate and up-to-date mapping and monitoring of rubber plantations can help understand regional LULC and their eco-environmental effects, and it supports land management and decision making [58]. Our study showed that the rubber plantation area in Xishuangbanna increased from 1987 to 2020. The change of rubber plantation can be divided into three stages. From 1987 to 2000, the growth rate of rubber plantations was relatively slow (see Fig. 8). This change might be that rubber was mostly planted on state farms at the time [54]. Since the land tenure reform in the 1980s, not only state-owned farms but also rubber plantations of small farmers have flourished [53]. From 2000 to 2010, the growth rate became faster due to China's further liberalization of trade controls on domestic natural rubber production. This finding was in consistent with [53], who reported that the rubber plantation in Xishuangbanna was developing rapidly because of the government incentive policy and the rising prices of natural rubber. However, we found that the rubber plantation area had been expanding slowly since 2010, probably due to the rubber prices had fallen steeply. According to the previous study the price of natural rubber latex sharply dropped to half of its historical peak since 2012 [59], [60], our results further supported these findings. In addition, China has gradually strengthened its understanding of the ecological environment and biodiversity protection, avoiding the ecological imbalance caused by a single species and further restricting the planting of rubber plantations.

Spatially, we found that the Xishuangbanna rubber forest was mainly concentrated in Jinghong City and Mengla County (see Fig. 9), which was similar to the results of previous [5], [51], [61]. Since 2000, rubber plantations in Xishuangbanna have expanded rapidly, especially on the Chinese side of the

borders with Laos and Myanmar. This might be due to the large demand for rubber, government support, and advances in agricultural technology [5]. An alternative explanation is geopolitical cooperation and government policies, such as the alternative development in the 1990s [9]. For example, in order to curb and reduce the sources of drugs and eliminate poppy cultivation, the governments of Myanmar and Laos have made rubber plantations the main alternative land use type [53]. Compared with Jinghong City and Mengla County, the rubber planting area in Menghai County has little change. This could be due to regional differences. Previous studies indicated that the average elevation of Menghai County is 1411.77 m, which is not suitable for rubber planting [62]. In addition, the expansion pattern of rubber plantations on Xishuangbanna was quite different from that of Hainan Island, the rapid expansion of rubber plantation on Hainan Island began in the early 1980s [63]. During the 1990s, rubber plantations on Hainan Island grew at a very low and stable speed. This difference may be related to China's Reform and Opening policy [64].

C. Uncertainties for Mapping Rubber Plantation

The extraction accuracy for rubber plantations is the premise and basis of evaluating data application. Theoretically, our classification results showed that both overall accuracy and Kappa values were reasonable, and the average overall accuracy was above 80%, while Kappa was above 0.75. However, as [65] reported that the kappa coefficient is not an index of accuracy, indeed it is not an index of overall agreement but one of agreement beyond chance. Therefore, we found errors in rubber classification in some areas through visual interpretation. This mainly occurred through rubber misclassification and omission in the early steps of the rubber plantation. The spatial distribution of misclassified points in rubber plantation areas was analyzed. It was found that most of the misclassified points in rubber plantations were classified as natural forests because there were many rubber plantations scattered in the study area, which had no obvious boundary with other forest covers around them, resulting in a decline of classification accuracy. In addition, in phenological analysis, remote sensing images show that neither leaf-off nor leaf-on processes may occur perfectly synchronously across the region. This change may be due to the long-time interval of Landsat images, the rubber phenological feature information is weakened in the data mosaic process.

We also conduct a comparative analysis of the monitored rubber plantation area and other sources such as the other scholar's related research and statistical yearbooks. We estimated that the area of rubber plantation in the study is much larger than that in the official statistics (see Table IV). In comparison, our results are closer to the [9], [51], and [52], which estimated that the area of rubber plantations in Xishuangbanna reached 50.10×10^4, 47.33×10^4, and 49.00×10^4 hm^2 in 2010, respectively. The difference between our results and the official statistics is likely caused by the underreporting of rapidly growing and relatively scattered small rubber plantations in the private sector. It can be inferred from this that official statistics underestimate the area expansion rate of rubber plantations in the study area.

VI. Conclusion

This article is based on the GEE platform using dense time stacking of time-series Landsat images and the RF algorithm to monitor the temporal–spatial changes of rubber forests in Xishuangbanna over the past 30 years. The results demonstrated that the overall accuracy values of the classification model from 1987 to 2020 ranged from 0.82 to 0.96, while Kappa values ranged from 0.76 to 0.95, indicating that the extraction accuracy can be considered reliable. The area of rubber plantations continuously expanded from 1987 to 2020, attaining a maximum value of 49.60×10^4 hm^2 in 2015. The Xishuangbanna rubber plantations are mainly located in Mongla County and Jinhong City, and its area has grown rapidly from 1987 to 2020. The distribution of rubber plantations in Menghai County is small and the area changes little.

However, there are several critical uncertainties and implications for further studies. A problem with the monitoring method due to the distribution and elevation of the study area is that defoliated rubber will appear asynchronously defoliated on remote sensing images in terms of temporal, and the timing of green leaves may also be asynchronous during the leaf-on period. Second, because the Landsat data has a long-time interval, the rubber phenology characteristic information is weakened in the process of data mosaic production. In the future, we suggest further exploration of this topic using multisource remote sensing image data fusion technology, including image fusion of MODIS and Landsat. In addition, given the changes in the phenological characteristics of rubber forests in different regions, the impact of terrain and climate on rubber forests requires further consideration. Extraction methods of rubber forest area also need to be discussed in combination with other approaches, such as maximum likelihood, support vector machine, artificial neural network, and deep learning algorithms [66]–[68]. In summary, despite these limitations, this article method provides an important reference for monitoring the distribution of rubber in other tropical regions.

Acknowledgment

The authors would like to thank all the staff members of the Google Earth Engine and Google Collaboratory. We also thank the editors and anonymous reviewers for their useful comments and suggestions on this article. In addition, we also have would like to thank the Kunming Municipal Commerce Bureau and Kunming Association of Foreign Economic and Technical Cooperation for their assistance in data acquisition.

References

[1] A. Ahrends *et al.*, "Current trends of rubber plantation expansion may threaten biodiversity and livelihoods," *Glob. Environ. Change-Hum. Policy Dimension*, vol. 34, pp. 48–58, Sep. 2015.

[2] X. Gong, "The role of Chinese corporate players in China's South China Sea policy," *Contemporary Southeast Asia*, vol. 40, no. 2, pp. 301–326, Aug. 2018.

[3] S. P. Gao, X. L. Liu, Y. C. Bo, Z. T. Shi, and H. M. Zhou, "Rubber identification based on blended high spatio-temporal resolution optical remote sensing data: A case study in Xishuangbanna," *Remote Sens.*, vol. 11, no. 5, Mar. 2019, Art. no. 496.

[4] Z. Hemati, S. Selvaraj, X. Shangwen, and X. Yang, "Identification of indicators: Monitoring the impacts of rubber plantations on soil quality in Xishuangbanna, Southwest China," *Ecol. Indicators*, vol. 116, 2020, Art. no. 106491.

[5] C. W. Xiao, P. Li, Z. M. Feng, and X. N. Liu, "An updated delineation of stand ages of deciduous rubber plantations during 1987–2018 using landsat-derived bi-temporal thresholds method in an antichronological strategy," *Int. J. Appl. Earth Observ. Geoinf.*, vol. 76, pp. 40–50, Apr. 2019.

[6] C. C. Zhang *et al.*, "Effect of textural features in remote sensed data on rubber plantation extraction at different levels of spatial resolution," *Forests*, vol. 11, no. 4, Apr. 2020, Art. no. 399.

[7] L. Dong, J. Tong, and C. Wang, "The application of airborne remote sensing technology in land and resources," *Appl. Mech. Mater.*, vol. 644–650, pp. 4360–4363, 2014.

[8] C. Liao, P. Li, Z. Feng, and J. Zhang, "Area monitoring by remote sensing and spatiotemporal variation of rubber plantations in Xishuangbanna," *Nongye Gongcheng Xuebao/Trans. Chin. Soc. Agricultural Eng.*, vol. 30, no. 22, pp. 170–180, Nov. 2014.

[9] X. Liu *et al.*, "Rubber plantation and its relationship with topographical factors in the border region of China, Laos and Myanmar," *J. Geogr. Sci.*, vol. 23, pp. 1019–1040, Oct. 2013.

[10] S. Gao, X. Liu, Y. Bo, Z. Shi, and H. Zhou, "Rubber identification based on blended high spatio-temporal resolution optical remote sensing data: A case study in Xishuangbanna," *Remote Sens.*, vol. 11, no. 5, Mar. 2019, Art. no. 496.

[11] J. Liu, T. Yunhong, and J. W. F. Slik, "Topography related habitat associations of tree species traits, composition and diversity in a Chinese tropical forest," *Forest Ecol. Manage.*, vol. 330, pp. 75–81, Oct. 2014.

[12] H. Fan, X. H. Fu, Z. Zhang, and Q. Wu, "Phenology-based vegetation index differencing for mapping of rubber plantations using Landsat OLI data," *Remote Sens.*, vol. 7, no. 5, pp. 6041–6058, May 2015.

[13] A. C. Xavier, B. F. T. Rudorff, L. M. S. Berka, and M. A. Moreira, "Multi-temporal analysis of MODIS data to classify sugarcane crop," *Int. J. Remote Sens.*, vol. 27, no. 4, pp. 755–768, Feb. 2006.

[14] C. L. Sun, Y. Bian, T. Zhou, and J. L. Pan, "Using of multi-source and multi-temporal remote sensing data improves crop-type mapping in the subtropical agriculture region," *Sensors*, vol. 19, no. 10, May 2019, Art. no. 2401.

[15] C. L. Liu, W. L. Li, G. F. Zhu, H. K. Zhou, H. P. Yan, and P. F. Xue, "Land use/land cover changes and their driving factors in the northeastern Tibetan plateau based on geographical detectors and Google Earth Engine: A case study in Gannan prefecture," *Remote Sens.*, vol. 12, no. 19, Oct. 2020, Art. no. 3139.

[16] L. L. Coulter *et al.*, "Classification and assessment of land cover and land use change in Southern Ghana using dense stacks of Landsat 7 ETM + imagery," *Remote Sens. Environ.*, vol. 184, pp. 396–409, Oct. 2016.

[17] P. Teluguntla *et al.*, "A 30-m landsat-derived cropland extent product of Australia and China using random forest machine learning algorithm on Google Earth Engine cloud computing platform," *ISPRS J. Photogramm. Remote Sens.*, vol. 144, pp. 325–340, Oct. 2018.

[18] N. Gorelick, M. Hancher, M. Dixon, S. Ilyushchenko, D. Thau, and R. Moore, "Google Earth Engine: Planetary-scale geospatial analysis for everyone," *Remote Sens. Environ.*, vol. 202, no. 3, pp. 18–27, Dec. 2017.

[19] L. Zhong, L. Yu, L. Xuecao, L. Hu, and P. Gong, "Rapid corn and soybean mapping in U.S. corn belt and neighboring areas," *Sci. Rep.*, vol. 6, no. 1, Nov. 2016.

[20] J. Wang *et al.*, "Mapping sugarcane plantation dynamics in Guangxi, China, by time series Sentinel-1, Sentinel-2 and Landsat images," *Remote Sens. Environ.*, vol. 247, Sep. 2020, Art. no. 111951.

[21] W. L. Li, P. F. Xue, C. L. Liu, H. P. Yan, G. F. Zhu, and Y. P. Cao, "Monitoring and landscape dynamic analysis of alpine wetland area based on multiple algorithms: A case study of Zoige plateau," *Sensors*, vol. 20, no. 24, Dec. 2020, Art. no. 7315.

[22] K. K. Liyanage *et al.*, "Evaluation of key meteorological determinants of wintering and flowering patterns of five rubber clones in Cishuangbanna, Yunnan, China," *Int. J. Biometeorol.*, vol. 63, no. 5, pp. 617–625, May 2019.

[23] I. Fernandez and N. Morales San Martin, "One-class land-cover classification using maxent: The effect of modelling parameterization on classification accuracy," *Peer J.*, vol. 7, May 2019, Art. no. e7016.

[24] C. Wang, Q. Gao, and M. Yu, "Quantifying trends of land change in Qinghai-Tibet plateau during 2001–2015," *Remote Sens.*, vol. 11, no. 20, Oct. 2019, Art. no. 2435.

[25] H. Wang *et al.*, "Impacts of topography on the land cover classification in the Qilian mountains, northwest China," *Can. J. Remote Sens.*, vol. 46, no. 3, pp. 1–16, 2020.

[26] J. Penuelas, T. Rutishauser, and I. Filella, "Phenology feedbacks on climate change," *Science*, vol. 324, no. 5929, pp. 887–888, May 2009.

[27] A. D. Richardson, T. F. Keenan, M. Migliavacca, Y. Ryu, O. Sonnentag, and M. Toomey, "Climate change, phenology, and phenological control of vegetation feedbacks to the climate system," *Agricultural Forest Meteorol.*, vol. 169, pp. 156–173, Feb. 2013.

[28] J. Guyot, V. Condina, F. Doare, C. Cilas, and I. Sache, "Role of ascospores and conidia in the initiation and spread of South American leaf blight in a rubber tree plantation," *Plant Pathol.*, vol. 63, no. 3, pp. 510–518, Jun. 2014.

[29] J. Rouse, R. Haas, J. Schell, D. Deering, and J. Harlan, "Monitoring the vernal advancement and retrogradation (green wave effect) of natural vegetation," NASA/GSFC Type III, Final Report, Jan. 1974.

[30] C. Tucker, "Red and photographic infrared linear combinations for monitoring vegetation," *Remote Sens. Environ.*, vol. 8, pp. 127–150, Jun. 1979.

[31] C. Jordan, "Derivation of leaf-area index from quality of light on the forest floor," *Ecology*, vol. 50, no. 4, pp. 663–666, Jul. 1969.

[32] S. K. McFeeters, "The use of the normalized difference water index (NDWI) in the delineation of open water features," *Int. J. Remote Sens.*, vol. 17, no. 7, pp. 1425–1432, May 1996.

[33] B. C. Gao, "NDWI—A normalized difference water index for remote sensing of vegetation liquid water from space," *Remote Sens. Environ.*, vol. 58, no. 3, pp. 257–266, Dec. 1996.

[34] X. M. Xiao *et al.*, "Modeling gross primary production of temperate deciduous broadleaf forest using satellite images and climate data," *Remote Sens. Environ.*, vol. 91, no. 2, pp. 256–270, May 2004.

[35] W. Ping, Z. Zhaokun, F. Hui, and Z. Zhiling, "The automatic extraction of road information by the technology of object-oriented," *Open Automat. Control Syst. J.*, vol. 7, pp. 1842–1847, Oct. 2015.

[36] J. Y. Yuan, D. L. Wang, and R. X. Li, "Remote sensing image segmentation by combining spectral and texture features," *IEEE Trans. Geosci. Remote Sens.*, vol. 52, no. 1, pp. 16–24, Jan. 2014.

[37] L. Journaux, M. F. Destain, J. Miteran, A. Piron, and F. Cointault, "Texture classification with generalized fourier descriptors in dimensionality reduction context: An overview exploration," in *Proc. Artif. Neural Netw. Pattern Recognit., Proc., Lecture Notes Artif. Intell.*, 2008, pp. 280–291.

[38] H. B. Huang *et al.*, "Mapping major land cover dynamics in Beijing using all Landsat images in Google Earth Engine," *Remote Sens. Environ.*, vol. 202, pp. 166–176, Dec. 2017.

[39] C. Pelletier, S. Valero, J. Inglada, N. Champion, and G. Dedieu, "Assessing the robustness of random forests to map land cover with high resolution satellite image time series over large areas," *Remote Sens. Environ.*, vol. 187, pp. 156–168, Dec. 2016.

[40] L. Breiman, "Random forests," *Mach. Learn.*, vol. 45, no. 1, pp. 5–32, Oct. 2001.

[41] V. Rodriguez-Galiano, B. Ghimire, J. Rogan, M. Chica-Olmo, and J. Rigol-Sanchez, "An assessment of the effectiveness of a random forest classifier for land-cover classification," *ISPRS J. Photogramm. Remote Sens.*, vol. 67, pp. 93–104, Jan. 2012.

[42] P. Y. Hao, Y. L. Zhan, L. Wang, Z. Niu, and M. Shakir, "Feature selection of time series MODIS data for early crop classification using random forest: A case study in Kansas, USA," *Remote Sens.*, vol. 7, no. 5, pp. 5347–5369, May 2015.

[43] T. Bylander, "Estimating generalization error on two-class datasets using out-of-bag estimates," *Mach. Learn.*, vol. 48, no. 1–3, pp. 287–297, Jul. 2002.

[44] G. Martínez-Muñoz and A. Suárez, "Out-of-bag estimation of the optimal sample size in bagging," *Pattern Recognit.*, vol. 43, no. 1, pp. 143–152, Jan. 2010.

[45] G. Y. Zhang, C.-X. Zhang, and J.-S. Zhang, "Out-of-bag estimation of the optimal hyperparameter in subbag ensemble method," *Commun. Statist. - Simul. Comput.*, vol. 39, no. 10, pp. 1877–1892, Oct. 2010.

[46] S. B. Sun *et al.*, "Mapping coastal wetlands of the Bohai rim at a spatial resolution of 10 m using multiple open-access satellite data and terrain indices," *Remote Sens.*, vol. 12, no. 24, Dec, 2020, Art. no. 4114.

[47] L. Zhang, Z. Gong, Q. Wang, D. Jin, and X. Wang, "Wetland mapping of Yellow River Delta wetlands based on multi-feature optimization of Sentinel-2 images," *Yaogan Xuebao/J. Remote Sens.*, vol. 23, pp. 313–326, Mar. 2019.

[48] R. Pontius and M. Millones, "Death to Kappa: Birth of quantity disagreement and allocation disagreement for accuracy assessment," *Int. J. Remote Sens.*, vol. 32, no. 15, pp. 4407–4429, Aug. 2011.

[49] A. R. Feinstein and D. V. Cicchetti, "High agreement but low Kappa: I the problems of two paradoxes," *J. Clin. Epidemiol.*, vol. 43, no. 6, pp. 543–549, Jan. 1990.
[50] D. V. Cicchetti and A. R. Feinstein, "High agreement but low kappa: II. Resolving the paradoxes," *J. Clin. Epidemiol.*, vol. 43, no. 6, pp. 551–558, Jan. 1990.
[51] C. Liu, J. Zhang, Y. Li, and X. Yang, "Rubber plantation of Xishuangbanna information extraction and monitoring of spatial-temporal pattern expansion," *J. Fujian Forestry Sci. Technol.*, vol. 44, no. 02, pp. 43–50, 2017.
[52] W. Kou, J. Dong, X. Xiao, A. Hernandez, and J. Qin, "Expansion dynamics of deciduous rubber plantations in Xishuangbanna, China during 2000–2010," *Gisci. Remote Sens.*, vol. 55, no. 6, pp. 905–925, 2018.
[53] C. Xiao, P. Li, and Z. Feng, "Monitoring annual dynamics of mature rubber plantations in Xishuangbanna during 1987–2018 using Landsat time series data: A multiple normalization approach," *Int. J. Appl. Earth Observ. Geoinf.*, vol. 77, pp. 30–41, May. 2019.
[54] H. Cao *et al.*, "Urban expansion and its impact on the land use pattern in Xishuangbanna since the reform and opening up of China," *Remote Sens.*, vol. 9, no. 2, Feb, 2017, Art. no. 137.
[55] F. Zhao, L. Zhang, Z. Xu, and D. F. Scott, "Evaluation of methods for estimating the effects of vegetation change and climate variability on streamflow," *Water Resour. Res.*, vol. 46, no. 3, pp. 742–750, 2010.
[56] Y. Lin *et al.*, "Pattern and driving factor of intense defoliation of rubber plantations in SW China," *Ecol. Indicators*, vol. 94, no. 1, pp. 104–116, Jun. 2018.
[57] K. K. Liyanage *et al.*, "Evaluation of key meteorological determinants of wintering and flowering patterns of five rubber clones in Xishuangbanna, Yunnan, China," *Int. J. Biometeorol.*, vol. 63, no. 5, pp. 617–625, May 2019.
[58] C. Senf, D. Pflugmacher, S. van der Linden, and P. Hostert, "Mapping rubber plantations and natural forests in Xishuangbanna (Southwest China) using multi-spectral phenological metrics from MODIS time series," *Remote Sens.*, vol. 5, no. 6, pp. 2795–2812, Jun. 2013.
[59] X. Jianchu, "Land use transition in montane mainland southeast Asia ‖ the political, social, and ecological transformation of a landscape: The case of rubber in Xishuangbanna, China," *Mountain Res. Develop.*, vol. 26, no. 3, pp. 254–262, 2006.
[60] P. Li, J. H. Zhang, and Z. M. Feng, "Mapping rubber tree plantations using a Landsat-based phenological algorithm in Xishuangbanna, Southwest China," *Remote Sens. Lett.*, vol. 6, no. 1, pp. 49–58, 2015.
[61] J. Yu, F. T. Li, Y. Wang, Y. Lin, Z. W. Peng, and K. Cheng, "Spatiotemporal evolution of tropical forest degradation and its impact on ecological sensitivity: A case study in Jinghong, Xishuangbanna, China," *Sci. Total Environ.*, vol. 727, no. 4, Jul. 2020, Art. no. 138678.
[62] X. H. Huang *et al.*, "Spatial-temporal succession of the vegetation in Xishuangbanna, China during 1976–2010: A case study based on RS technology and implications for eco-restoration," *Ecol. Eng.*, vol. 70, pp. 255–262, Sep. 2014.
[63] B. Q. Chen *et al.*, "Identifying establishment year and pre-conversion land cover of rubber plantations on Hainan island, China using landsat data during 1987-2015," *Remote Sens.*, vol. 10, no. 8, Aug. 2018, Art. no. 1240.
[64] B. Q. Chen *et al.*, "Mapping tropical forests and deciduous rubber plantations in Hainan island, China by integrating PALSAR 25-m and multi-temporal Landsat images," *Int. J. Appl. Earth Observ. Geoinf.*, vol. 50, pp. 117–130, Aug. 2016.
[65] G. Foody, "Explaining the unsuitability of the kappa coefficient in the assessment and comparison of the accuracy of thematic maps obtained by image classification," *Remote Sens. Environ.*, vol. 239, Mar. 2020, Art. no. 111630.
[66] L. Ma *et al.*, "A review of supervised object-based land-cover image classification," *ISPRS J. Photogramm. Remote Sens.*, vol. 130, pp. 277–293, Aug. 2017.
[67] M. Sheykhmousa, M. Mahdianpari, H. Ghanbari, F. Mohammadimanesh, P. Ghamisi, and S. Homayouni, "Support Vector Machine Versus Random Forest for Remote Sensing Image Classification: A Meta-Analysis and Systematic Review," *IEEE J. Sel. Topics Appl. Earth Observ. Remote Sens.*, vol. 13, pp. 6308–6325, Sep. 2020.
[68] M. Amani, A. Ghorbanian, S. A. Ahmadi, M. Kakooei, A. Moghimi, S. M. Mirmazloumi, S. H. A. Moghaddam, S. Mahdavi, M. Ghahremanloo, S. Parsian, Q. S. Wu, and B. Brisco, "Google Earth Engine Cloud Computing Platform for Remote Sensing Big Data Applications: A Comprehensive Review," *IEEE J. Sel. Topics Appl. Earth Observ. Remote Sens.*, vol. 13, pp. 5326–5350, Sep. 2020.

Yuchen Li received the B.S. degree Geography from Handan College, Handan, China, in 2018, the M.S. degree in Cartography and Geographical Information System from Yunnan University, Kunming, China, in 2021, He is currently working toward the Ph.D. degree in Cartography and Geographical Information System from South China Normal University, Guangzhou, China.

His research interests include remote sensing of natural resources and environment, and coastal ecological environment monitoring.

Chenli Liu received the B.S. degree in Geographical Information System from Southwest Forestry University, Kunming, China, in 2015, the M.S. degree in Cartography and Geographical Information System from Yunnan University, Kunming, China, in 2018. He is currently working toward the Ph.D. degree in grassland science at Lanzhou University, Lanzhou, China.

His current research interests include remote sensing of grassland and ecological security.

Jun Zhang received the Ph.D. degree in cartography and geographic information system from Nanjing Normal University, Nanjing, China, in 2003.

He is currently an Associate Professor with the Cartography and Geographic Information System, Yunnan University, where he is also the Director of the Department of Geographic Information Science, Yunnan University. His research interests include remote sensing, geographic information system technologies, and applications in agriculture and the environment.

Ping Zhang received the B.S. degree in surveying and mapping engineering from Yunnan Normal University, Kunming, China, in 2019. She is currently working toward the M.S. degree in Cartography and Geography Information System at Yunnan University, Kunming, China.

Her current research interests include remote sensing information extraction, concentrating on coffee planting information extraction.

Yufei Xue received the B.S. degree in Geography Information Science from the College of Surveying, Mapping and Geographic Information, Shandong Jianzhu University, Jinan, China, in 2018. He is currently working toward the M.S. degree in Cartography and Geography Information System at Yunnan University, Kunming, China.

His current research interests include remote sensing information extraction, concentrating on tobacco planting information extraction, deep learning, GEE.